Electronic Supplementary Material (ESI) for CrystEngComm.

Supplementary Information

Generality of Liquid Precursor Phases in Gas Diffusion-Based Calcium Carbonate Synthesis

Maxim B. Gindele,[a] Luisa Vanessa Steingrube[a] and Denis Gebauer*,[a]

a. Institute of Inorganic Chemistry, Leibniz University Hannover, Callinstrasse 9, D-30167 Hannover, Germany; E-Mail: gebauer@acc.uni-hannover.de

Table of Contents

1. Carbonate free reference experiments 2
2. Manipulation of PAA stabilized $CaCO_3$ films 2
3. Characterization techniques 2
4. Supplementary Discussion 3
5. Figures 5
6. Legend for movies 16
7. References 16

Other supplementary materials for this Communication include the following:

Movies S1 to S3

1. Carbonate free reference experiments

Carbonate free experiments were carried out as reference experiments. In regular experiments,[1] $(NH_4)_2CO_3$ decomposes to CO_2 and NH_3 which then diffuse into the calcium chloride solutions raising the pH value. As raising the pH value will lead to deprotonation of PAA and possibly to the precipitation of coacervates,[2, 3] gas diffusion experiments with pure NH_3 were carried out to simulate the increase of pH in the solution in absence of CO_2. All solutions were prepared using Milli-Q water that was degassed by bubbling N_2 through the solution overnight. All solutions were stored and handled under nitrogen atmosphere during the execution of the experiments.

Glass wafers (5 x 5 mm) were placed on the bottom of a 200 mL round bottom flask that was flushed with N_2 for 10 minutes. Then, with the N_2 stream running, 20 µL of solutions containing $CaCl_2$ (20 mM) and different concentrations of PAA (0 g/L to 1 g/L) were placed on the wafers using an Eppendorf pipette. Next to the wafers, 0.5 g of ammonium nitrate was placed inside a small dish and 0.5 mL of 1 M NaOH (1 M stock solution, Roth) was added to the NH_4NO_3. Then, the N_2 stream was stopped and the flask closed. After the desired reaction time (1-5 h), the experiments were stopped, and the solutions were removed using a filter paper whilst still being under N_2 atmosphere. The wafers were dried in vacuum overnight and characterized using SEM (Fig. S1). No film was visible in any experiment, although for high polymer concentrations the solutions turned turbid.

2. Manipulation of PAA stabilized $CaCO_3$ films

Experiments were carried out to try to manipulate and isolate the PAA stabilized $CaCO_3$ film. Therefore, 1 h experiments with 20 mM $CaCl_2$ and 1.0 g/L PAA were carried out on glass wafers as described before. For these conditions, the film was visible by eye and manipulation of the film could be investigated using light microscopy (Supporting Movies S1 to S3).

3. Characterization techniques

SEM images in Fig. S2 and S10b-c were recorded using a JEOL JSM-6700F SEM without coating the sample prior to analysis.

4. Supplementary Discussion

It is demonstrated how the time of liquid-liquid phase separation (LLPS) in gas diffusion-based experiments can be estimated in case of the aqueous calcium carbonate system.

Previous results showed that the liquid-liquid binodal limit is defined by the solubility threshold of proto-structured ACCs.[4] In the following, it is assumed, that the pH value of the solution quickly reaches a constant value of 9.8 in the first few minutes after the start of the experiments, as previously established in ref.[5]

From the known starting concentration of $CaCl_2$ (10 mM) and the solubility product of ACC[6] (3.8×10^{-8} M^2) the amount of carbonate necessary to cross the binodal limit can be calculated according to (expressed in concentrations):[7]

$$c_{free}(CO_3^{2-}) = \frac{IAP(ACC)}{c_{free}(Ca^{2+})}$$

The calculated free carbonate concentration is $c_{free}(CO_3^{2-}) = 3.8\ \mu M$. From this carbonate concentration and the estimated carbonate addition rate $d[CO_3]/dt$ due to in-diffusion in the vapor diffusion experiment, we can estimate the time at which LLPS occurs.

Meldrum et. al. investigated the effects of different parameters on the gas diffusion.[5] They determined $d[CO_3]/dt$ to be linear dependent on the solution surface area, exponentially dependent on the cross sectional area of diffusion barriers and on the initial calcium concentrations, and independent of the amount of $(NH_4)_2CO_3$ used for the experiments. In addition, they provided carbonate addition rates for conditions similar to our experiments, with 25 mM $CaCl_2$ and a 2.6 dm^3 desiccator used for the gas diffusion experiments.

Based on these investigations, the carbonate addition rate was calculated. The surface area of the droplets was estimated using a hemispherical droplet with a radius of 2.5 mm. As described in SI section 1, two diffusion barriers were used in our experiments, the first barrier has 3 holes of 1 mm diameter and the second one has one hole of 0.1 mm diameter for each chamber. The cross-sectional area of the first barrier is therefore more than 2 orders of magnitude larger than the second barrier (2.4 mm^2 vs. 7.8×10^{-3} mm^2). Due to the exponential dependency of cross-sectional area and diffusion speed, the second diffusion barrier can be seen as the rate determining step in this system and the first barrier was not used for the calculations.

Using these assumptions, the provided general conditions, and the relationships of parameters and carbonate addition rate, we determine $d[CO_3]/dt = 0.14\ \mu M/min$. The diffusion of 3.8 µM carbonate in the droplet therefore roughly takes **28 minutes**.

Using this estimation, we predict that the phase-separation takes place on the timescale of minutes. It also agrees with our results, as no film was detected if experiments are stopped after 5 min (data not shown) and precursor films were detectable in 30-minute experiments (Fig. 3c in the main text).

5. Figures

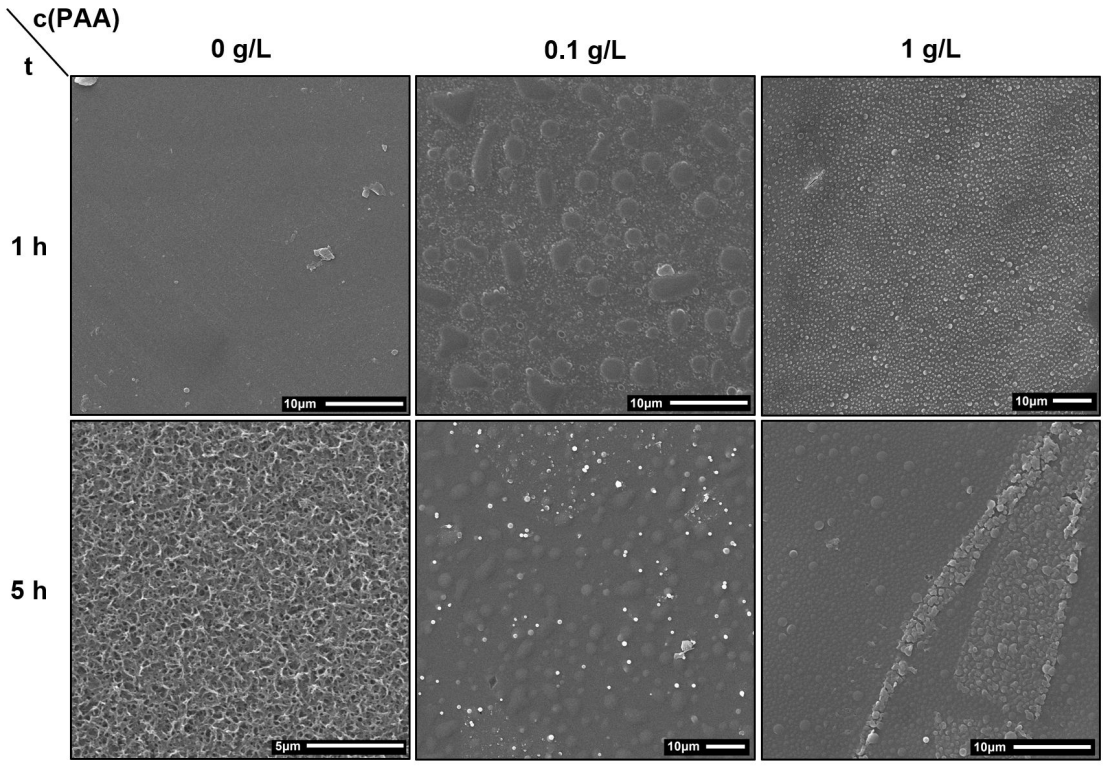

Fig S1. SEM characterization of carbonate free reference experiments (see SI section 1). Experiments were performed using 20 mM $CaCl_2$ concentrations and experiments were carried out for 1 h to 5 h. In the experiments, no film was detected, although for PAA concentrations higher than 0.01 g/L, the solution turned turbid, indicating the precipitation of a Ca-PAA coacervate. The precipitated coacervates possess a different structure compared to the species found in the regular experiments with carbonate, as they primarily form droplets with irregular shapes, instead of spherical particles or smooth films (Fig. S5). Therefore, for the PAA concentrations used in this work, the coprecipitation of coacervate cannot be excluded, but the primary phase in all cases is $CaCO_3$, as confirmed by ATR-IR (Fig. 2b in the main text), showing that the formation of coacervates only plays an insignificant role in this work.

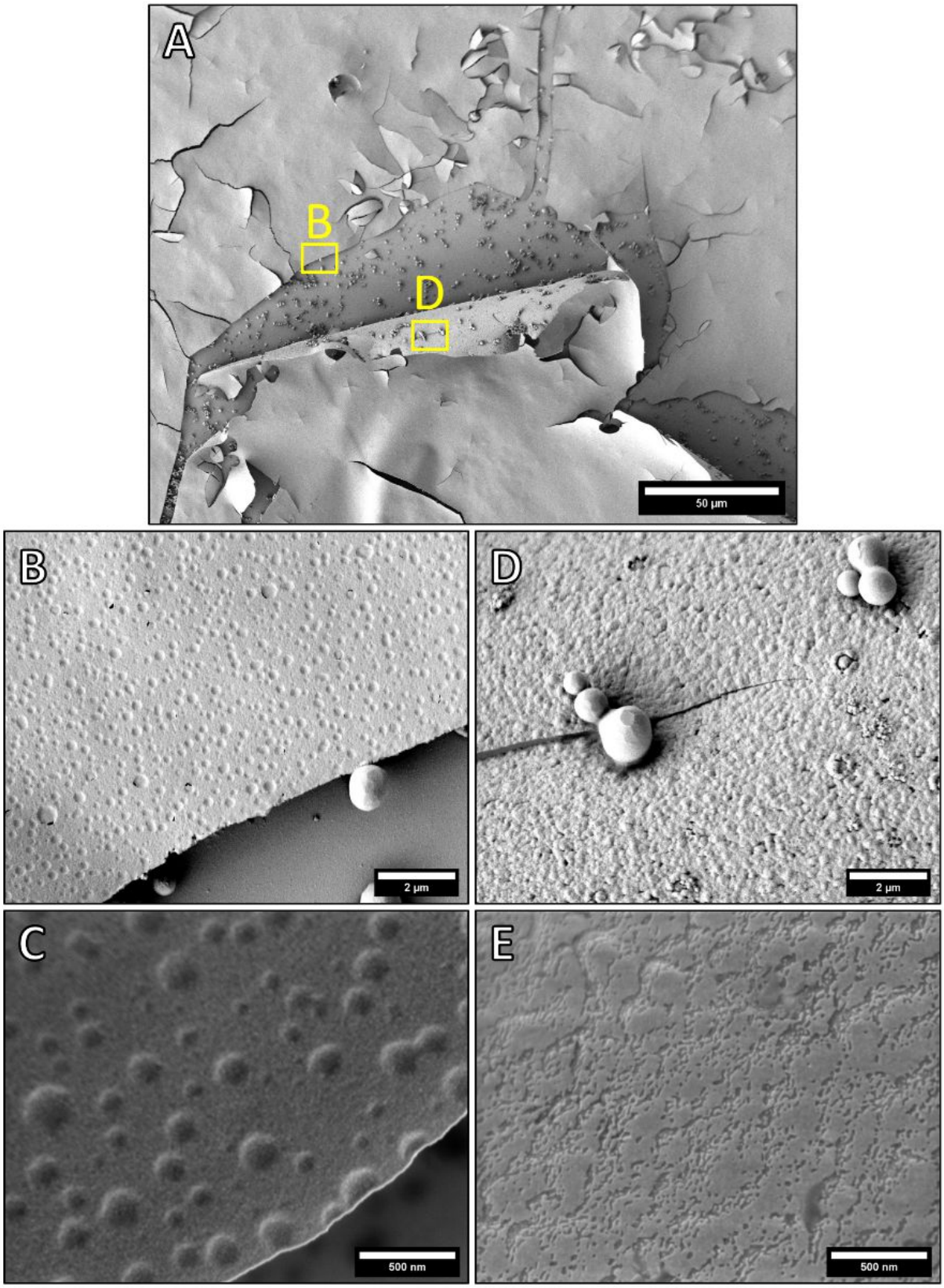

Fig S2. Higher resolution SEM images of the dried liquid precursor film. The difference in morphology of the top surface (B and C) and the bottom surface (D and E) of the film is visible. Experimental conditions: 2 h gas diffusion experiment using 20 mM $CaCl_2$ with 0.1 g/L PAA.

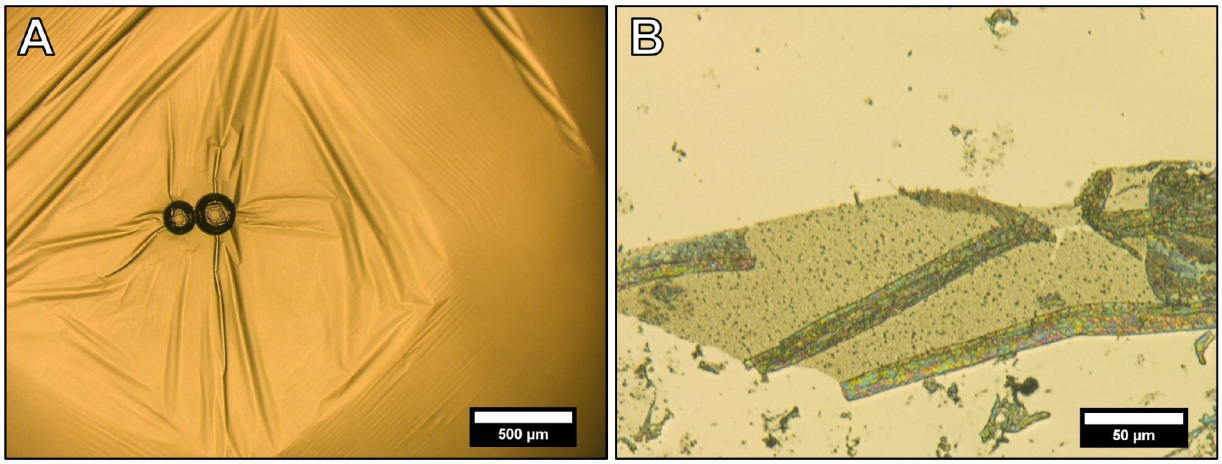

Fig S3. Light microscopy images for 1 h gas diffusion experiments. Images were taken before the solution was removed. A) Film in presence of 0.5 g/L PAA and 20 mM $CaCl_2$. If the film is manipulated it breaks apart into smaller fragments (Supporting Movie S1). B) Fragment of a broken film. Particles are visible in the structure once the film is broken up. It was not possible to isolate the film (Supporting Movie S2).

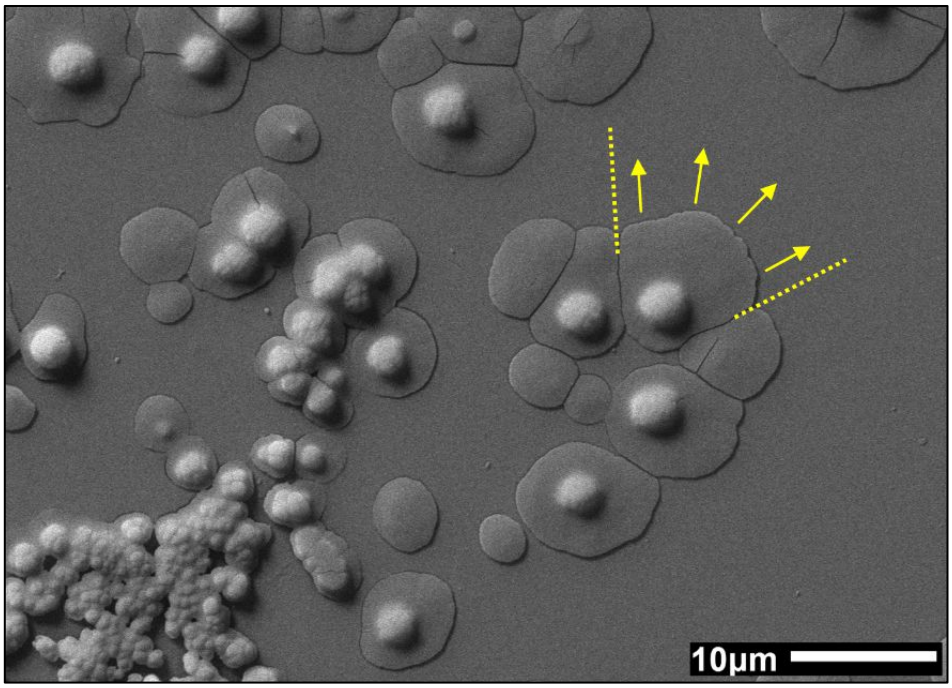

Fig S4. Precursor particles formed in 1 h gas diffusion experiment using 20 mM $CaCl_2$ and 0.01 g/L PAA. The picture shows dried residues of precursor droplets that precipitated onto the wafer. In several experiments, these droplets could be detected in addition to the films. Based on this, we are able to discuss whether the droplets are indeed liquid. Macroscopically, we can use the following definition for a liquid:[8] "When a substance conforms to the shape of its container without necessarily filling it, it is said to be in the liquid state." Using this macroscopic definition we can evaluate the shown SEM analysis. Due to the liquid character of the precursor droplets in the solution in their hydrated state, the droplets spread upon precipitation on the wafer. It is clear that the droplets spread out and conform to the shape of the container. If no material is besides the droplet, the droplets spread regularly and the liquid forms a circle around the droplet, if material had already precipitated besides the droplet, that material conforms to the set boundaries and flows in one direction, as indicated by the arrows. Using the macroscopic definition, the precursor phases would qualify as a liquid, at least on a µm scale (although the microscopic structure of the liquid precursor can be different).[9]

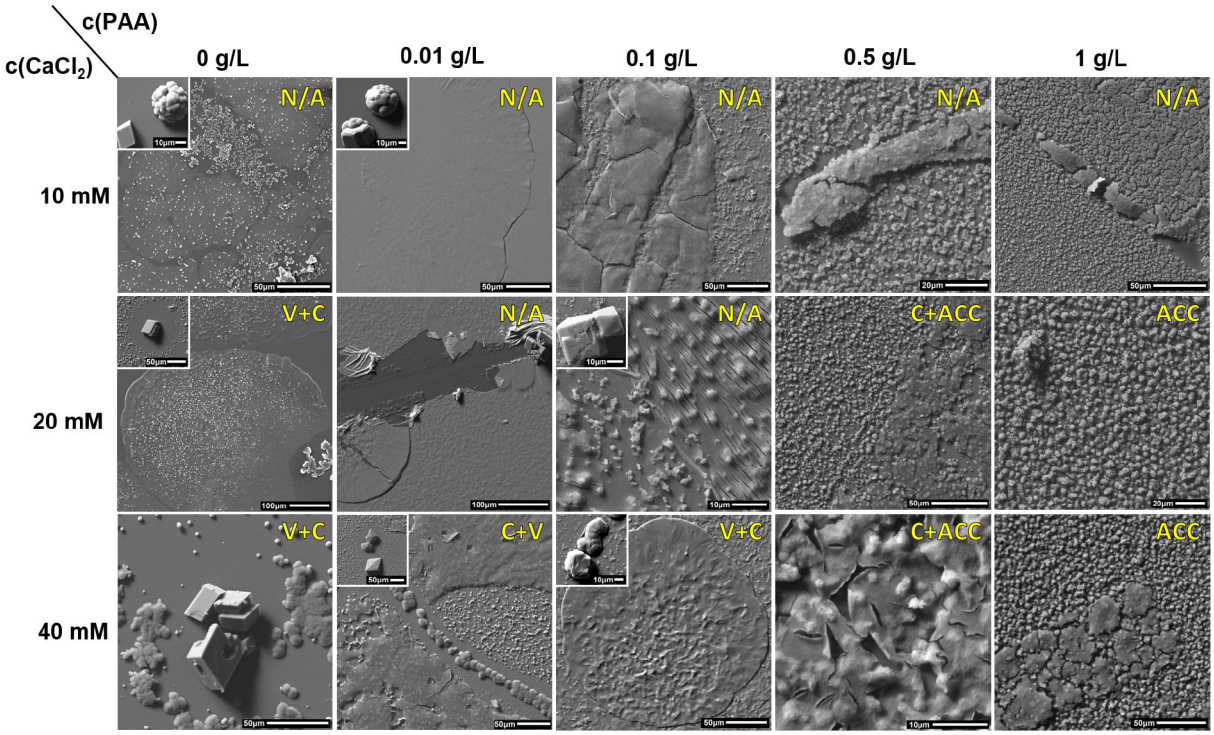

Fig S5. SEM images for 1 h gas diffusion experiments with varying $CaCl_2$ and PAA concentrations. For experiments with PAA, usually the whole wafer was covered with films or particles. If larger particles were observed as well, these are shown in the inset in the top left corner. In the top right corner, the polymorph determined by ATR-FTIR is stated (C: calcite; V: vaterite; ACC: amorphous calcium carbonate; N/A: not available). It was not possible to recorded IR spectra for all samples as the concentration of $CaCO_3$ on the wafers is very low, especially for experiments with 10 mM $CaCl_2$.

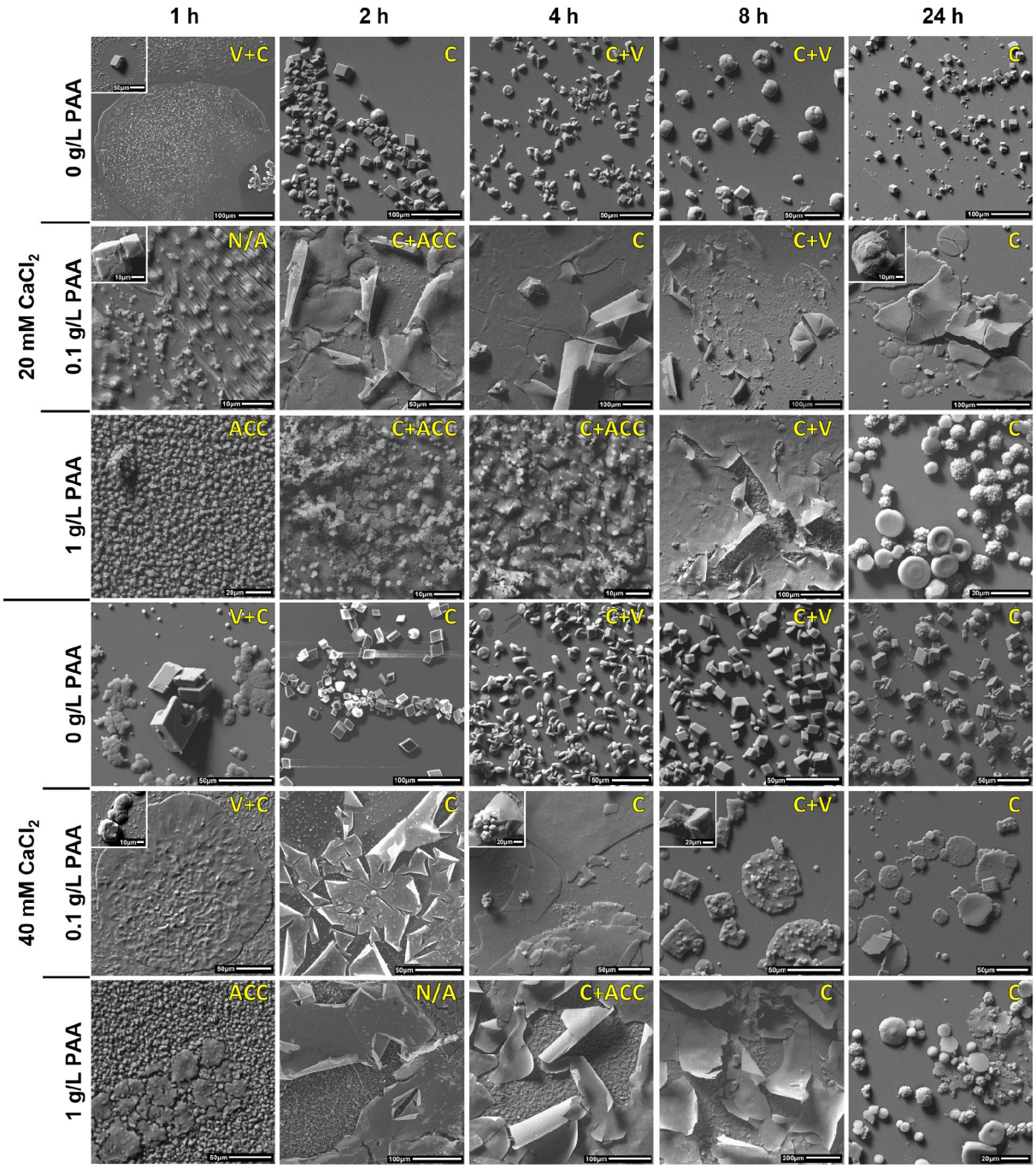

Fig S6. Time dependent gas diffusion experiments using different PAA concentrations. In the top right corner, the determined polymorph by ATR-FTIR is stated (C: calcite; V: vaterite; ACC: amorphous calcium carbonate; N/A: not available).

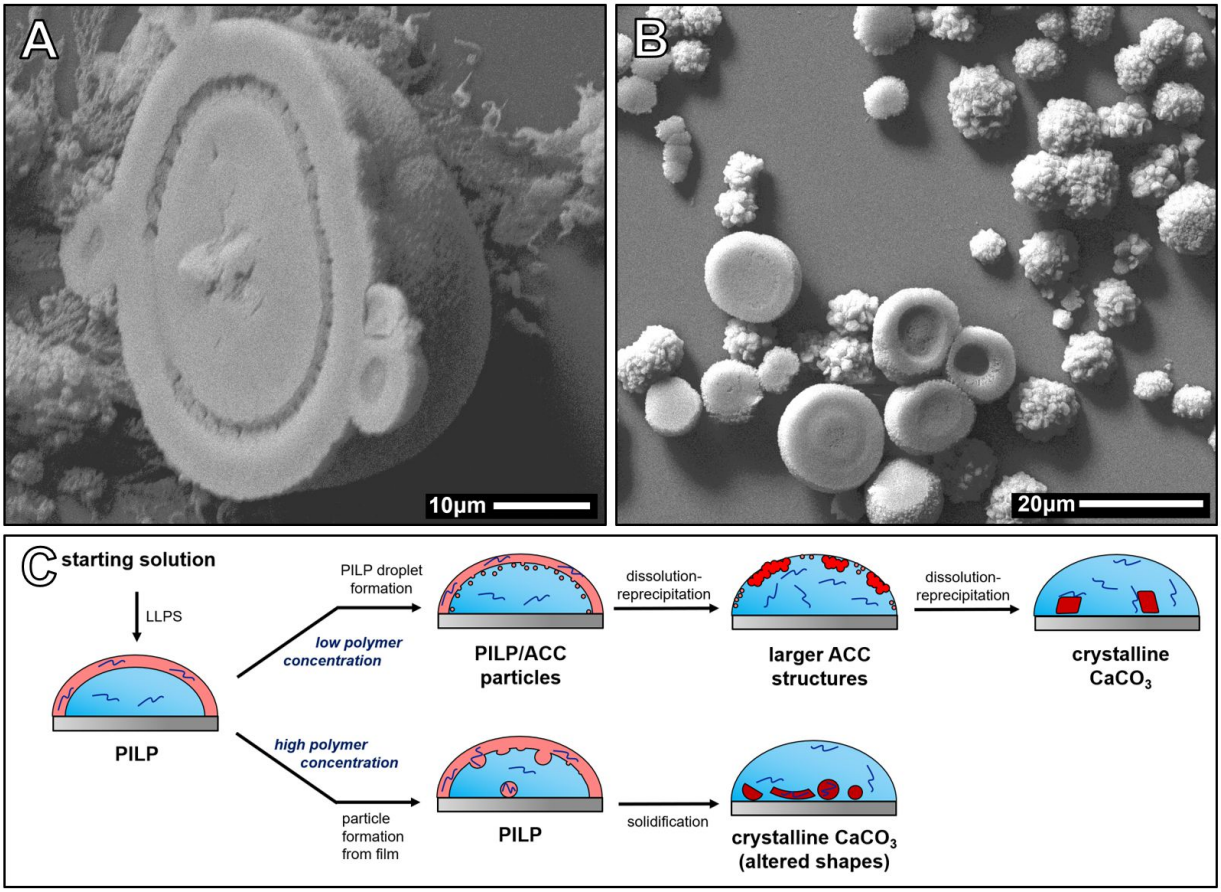

Fig S7. A) and B) SEM images of spherical particles in gas diffusion experiments with PAA. Experimental conditions: A) 8 h experiment with 10 mM $CaCl_2$ and 0.5 g/L PAA. B) 24 h gas diffusion experiment with 20 mM $CaCl_2$ and 1 g/L PAA. C) Proposed mechanism for crystallization in presence of PAA in gas diffusion experiments. Higher concentrations of polymer additives stabilize the liquid and amorphous phases, therefore preventing dissolution, resulting in formation of complex particle shapes from the liquid precursor (PILP) phase.

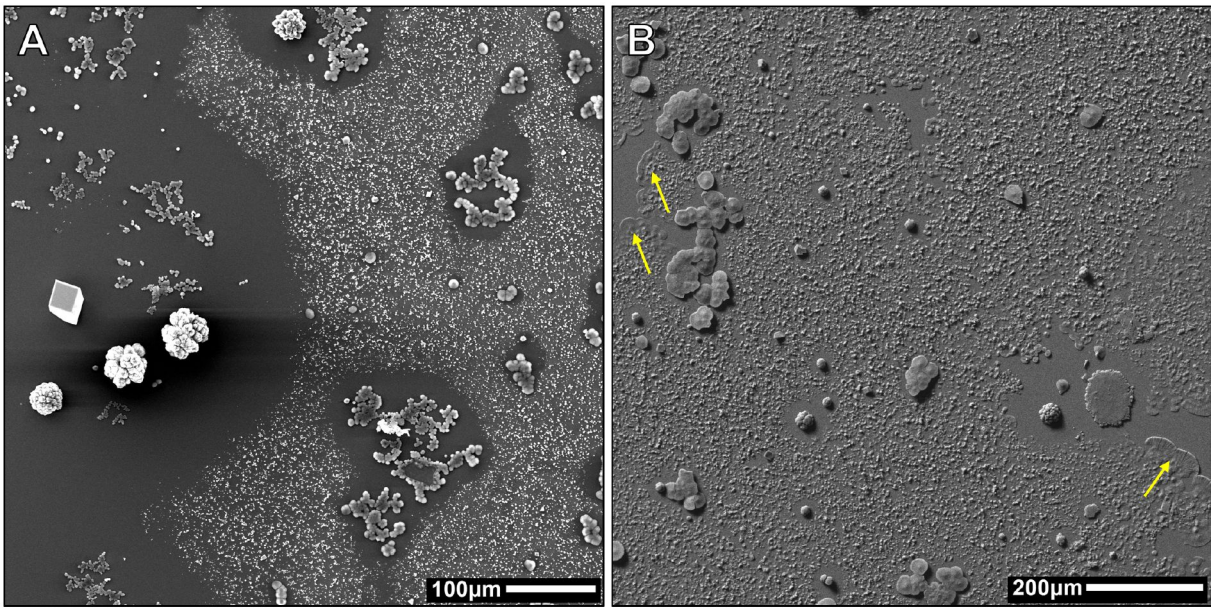

Fig S8. Overview images for the structures observed in 1 h additive-free gas diffusion experiments for $CaCl_2$ concentrations of A) 10 mM and B) 40 mM. As there are no films or smaller particles visible around the larger amorphous or crystalline structures, a dissolution-reprecipitation mechanism is expected. Continuous parts of the film are visible as well (arrows in B).

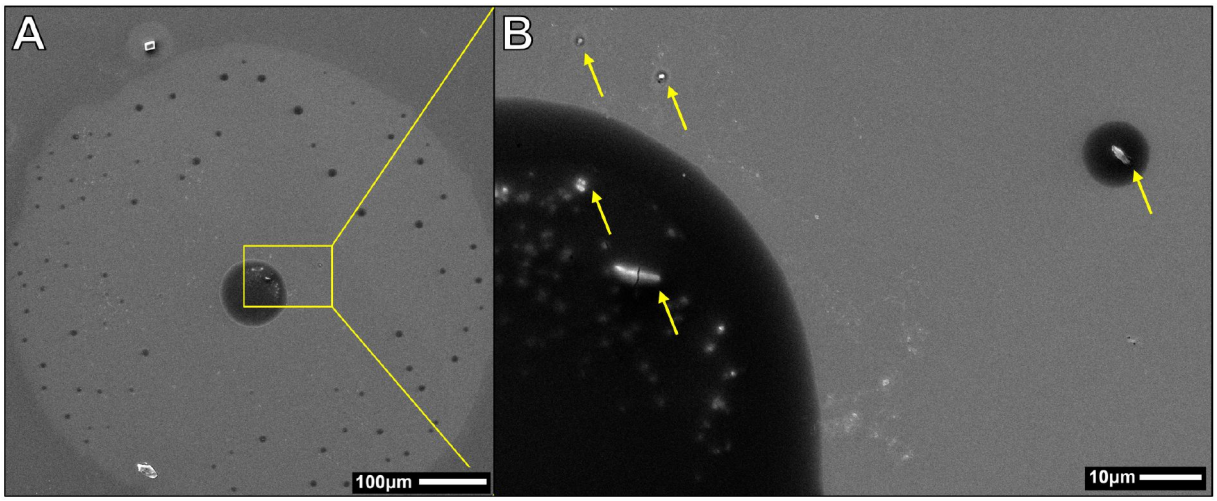

Fig S9. SEM images of a 30 min gas diffusion experiment using 10 mM $CaCl_2$. A) A large film with a diameter of 0.7 mm is visible, suspected to be the precursor to the films seen in 1 h experiments. B) Higher resolution image of the holes in the film. Inside the holes, particles are visible (arrows), indicating that this film is indeed a precursor to other solid species. The drastic difference in brightness of the holes compared to the film most likely arises from the densification of the film after the wafer was coated with gold for SEM analysis. This densification was most likely induced by the electron beam during analysis of the sample.

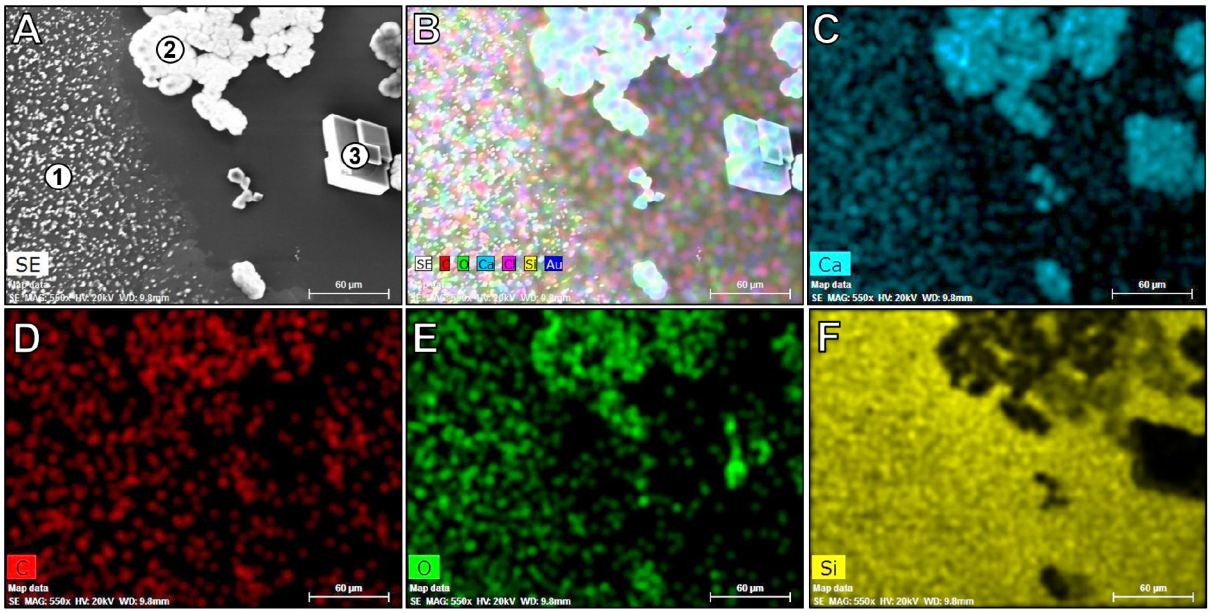

Fig S10. EDX characterization of different detected $CaCO_3$ species. A) Chosen area for mapping from an 1 h additive-free gas diffusion experiment using 20 mM $CaCl_2$. The film (1, film has already partially transformed to particles, as described in the main text), amorphous structures (2) and crystalline structures (3) are visible. B) Combined elemental mappings. C) to F) individual mappings for Ca, C, O and Si. It is evident, that all structures contain Ca, O and C. A quantitative EDX determination was not possible, as the film is very thin and mainly Si from the wafer beneath (F) was detected.

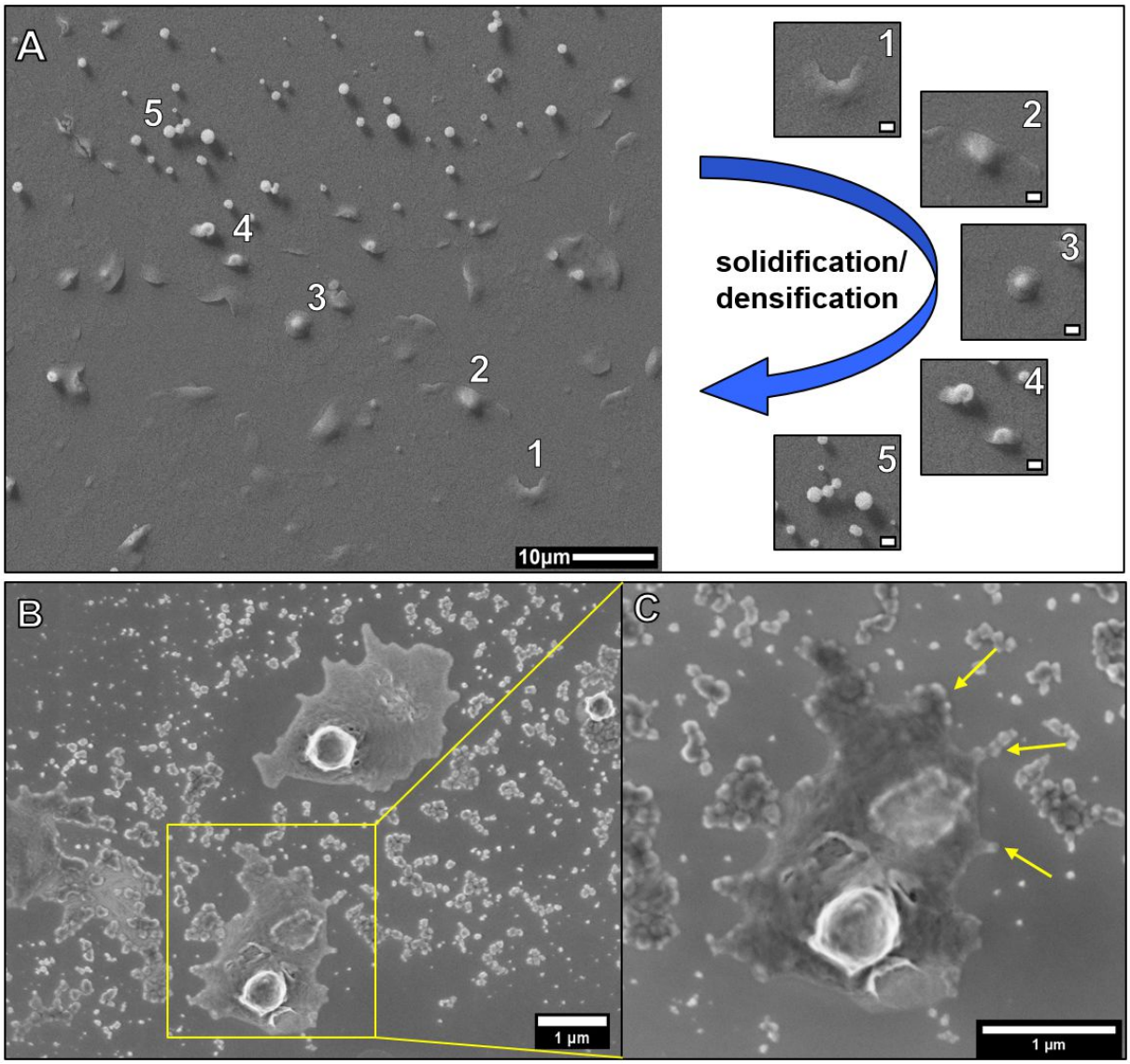

Fig S11. Transformation of the precursor film to particles. A) The transformation of the film to µm sized particles is captured in the image. Intermediate stages of the transformation are visible hinting towards a solidification/densification process instead of a dissolution-reprecipitation process. This most likely happens through dehydration of the dense liquid phases. Experimental conditions: 1 h gas diffusion experiment using 10 mM $CaCl_2$ without additive. Scale bar in insets 1 to 5 is 1 µm. B) and C) Higher resolution SEM images of the formation of a µm sized particle. Around the particles, films are visible that transform to 50 to 150 nm particles (yellow arrows). Experimental conditions: 1 h gas diffusion experiment using 20 mM $CaCl_2$ without additive.

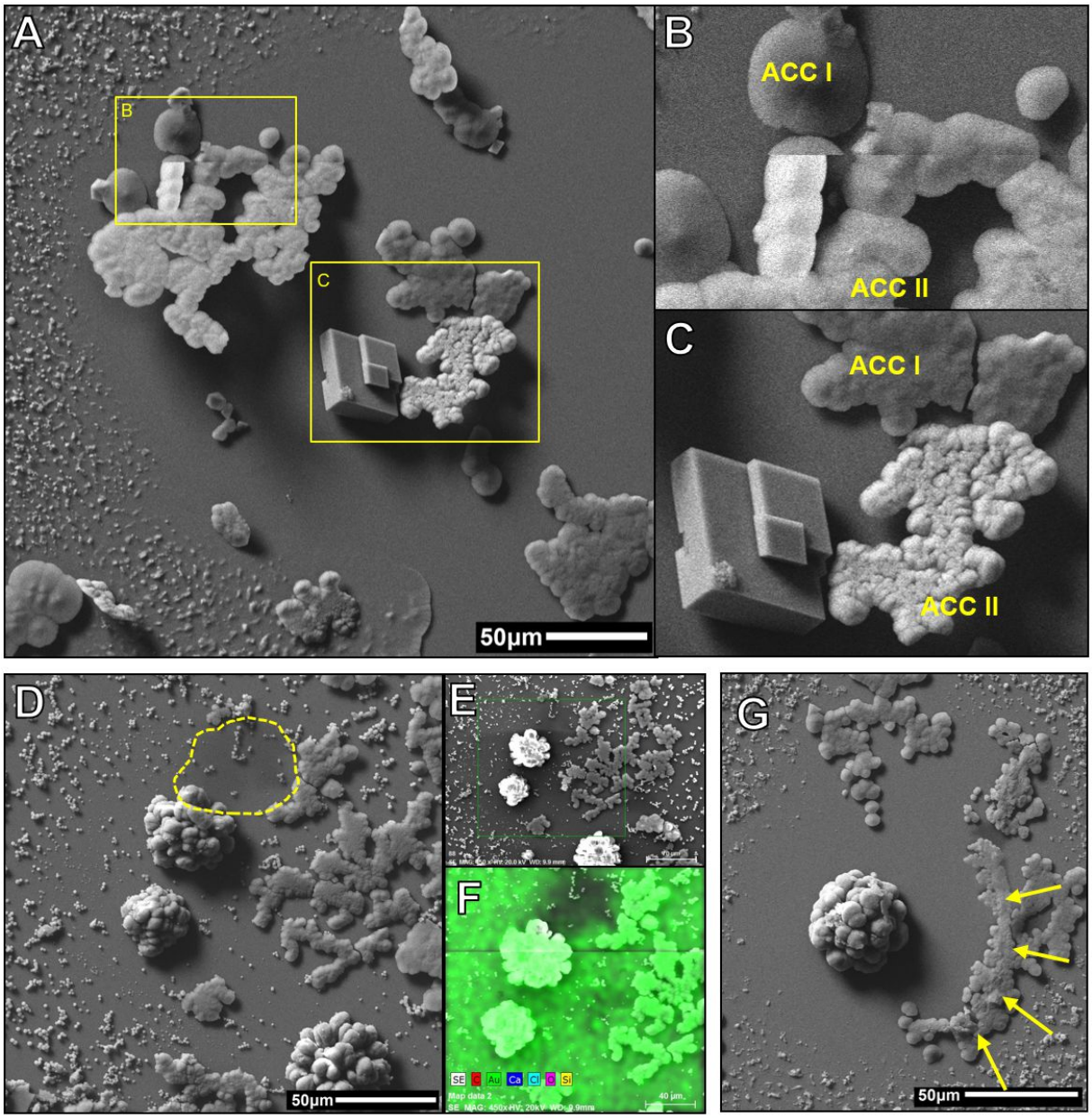

Fig S12. Transformation mechanisms for amorphous calcium carbonates induced by the electron beam during SEM investigations in additive-free experiments. A) Overview image for a 1 h gas diffusion experiment using 20 mM $CaCl_2$. Different amorphous and crystalline structures can be seen. B) Magnification of the transformation of one ACC phase (ACC I) into a second ACC phase (ACC II). Due to the decrease in size toward a smaller volume of the ACCII particles upon imaging (see the line in the middle of the image), the ACCII phase seems to possess a higher density. The solid-state transformation is very fast and finished within one recorded row of pixels (less than 0.1 s). C) ACC I and ACC II besides a calcite particle. The difference in structure and brightness (detected secondary electrons) between the ACC structures is obvious. The occurrence of different types of ACC was reported in the literature before.[10-14] D) Solid-state transformation of an amorphous precursor to vaterite. The transition could not be captured in an image but EDX (E and F) shows the lack of Au-coating at which the amorphous phase used to be (highlighted region in D). The densification of the phase is obvious as the area covered before transformation is much larger than afterwards. G) Evidence for a dissolution-reprecipitation mechanism of the transformation of amorphous structures to crystalline $CaCO_3$. The ACC phase dissolved in a circular fashion around a vaterite particle (arrows). The formation of a preferential polymorph (calcite vs. vaterite) via the crystallization of the different ACC phases (ACCI and ACCII) could not be observed.

6. Legend for movies

Movie S1 Manipulation of the PILP film with tweezers. It was not possible to isolate the thin, fragile film, as it broke apart into smaller fragments (Fig. S4b), which seemed to dissolve.

Movie S2 Attempt to isolate the PILP film using an Eppendorf pipette. It was not possible to isolate the film due to its thinness and fragility. The isolated solution was transferred to another wafer, but no $CaCO_3$ mineralization was observed, as the concentration of the precursor phase in the isolated solution was too low for sustaining liquid-liquid coexistence.

Movie S3 Film on surface of droplet with already precipitated PILP/ACC particles at the bottom of the wafer.

7. References

1. C. Ruiz-Agudo, J. Lutz, P. Keckeis, M. King, A. Marx and D. Gebauer, *J. Am. Chem. Soc.*, 2019, **141**, 12240-12245.
2. A. Ikegami and N. Imai, *J. Polym. Sci.*, 1962, **56**, 133-152.
3. L. Mureşan, P. Sinha, P. Maroni and M. Borkovec, *Colloids Surf. A Physicochem. Eng. Asp.*, 2011, **390**, 225-230.
4. F. Sebastiani, S. L. Wolf, B. Born, T. Q. Luong, H. Cölfen, D. Gebauer and M. Havenith, *Angew. Chem. Int. Ed.*, 2017, **56**, 490-495.
5. J. Ihli, P. Bots, A. Kulak, L. G. Benning and F. C. Meldrum, *Adv. Funct. Mater.*, 2013, **23**, 1965-1973.
6. D. Gebauer, A. Völkel and H. Cölfen, *Science*, 2008, **322**, 1819-1822.
7. M. Kellermeier, A. Picker, A. Kempter, H. Cölfen and D. Gebauer, *Adv. Mater.*, 2014, **26**, 752-757.
8. J. S. Rowlinson, F. L. S., *Liquids and Liquid Mixtures, 3rd Edition.* Butterworths: London, 1982.
9. Y. Xu, K. C. H. Tijssen, P. H. H. Bomans, A. Akiva, H. Friedrich, A. P. M. Kentgens and N. Sommerdijk, *Nat. Commun.*, 2018, **9**, 2582.
10. P. Bots, L. G. Benning, J.-D. Rodriguez-Blanco, T. Roncal-Herrero and S. Shaw, *Cryst. Growth Des.*, 2012, **12**, 3806-3814.
11. B. P. Pichon, P. H. Bomans, P. M. Frederik and N. A. Sommerdijk, *J. Am. Chem. Soc.*, 2008, **130**, 4034-4040.
12. D. Gebauer, P. N. Gunawidjaja, J. Y. P. Ko, Z. Bacsik, B. Aziz, L. Liu, Y. Hu, L. Bergström, C.-W. Tai, T.-K. Sham, M. Edén and N. Hedin, *Angew. Chem. Int. Ed.*, 2010, **49**, 8889-8891.
13. Y. Levi-Kalisman, S. Raz, S. Weiner, L. Addadi and I. Sagi, *Adv. Funct. Mater*., 2002, **12**, 43-48.
14. Y. Politi, R. A. Metzler, M. Abrecht, B. Gilbert, F. H. Wilt, I. Sagi, L. Addadi, S. Weiner and P. Gilbert, *Proc. Natl. Acad. Sci. U.S.A.*, 2008, **105**, 17362-17366.